New Journal of Physics
The open–access journal for physics

Direct determination of ultrafast intersubband hole relaxation times in voltage biased SiGe quantum wells by a density matrix interpretation of femtosecond resolved photocurrent experiments

P Rauter[1], T Fromherz[1], N Q Vinh[2], B N Murdin[3], J P Phillips[4], C R Pidgeon[4], L Diehl[5], G Dehlinger[5], D Grützmacher[5], Ming Zhao[6], Wei-Xin Ni[6] and G Bauer[1]

[1] Institute of Semiconductor and Solid State Physics, University of Linz, Austria
[2] FOM Institute for Plasma Physics, Rijnhuizen, Nieuwegein, The Netherlands
[3] University of Surrey, Guildford, UK
[4] Heriot-Watt University, Edinburgh, UK
[5] Paul Scherrer Institut, Villingen, Switzerland
[6] University of Linkoeping, Linkoeping, Sweden
E-mail: patrick.rauter@jku.at

New Journal of Physics **9** (2007) 128
Received 12 February 2007
Published 17 May 2007
Online at http://www.njp.org/
doi:10.1088/1367-2630/9/5/128

Abstract. We report the quantitative and direct determination of hole intersubband relaxation times in a voltage biased SiGe heterostructure using density matrix calculations applied to a four-level system in order to interpret photocurrent (PC) pump–pump experiments. One consistent set of parameters allows the simulation of two kinds of experiments, namely pump–pump photocurrent experiments at a free electron laser (wavelength 7.9 μm) and the laser-power dependence of the PC signal. This strongly confirms the high reliability of these parameter values, of which the most interesting in respect to Si based quantum cascade laser development is the extracted heavy-hole relaxation time. The simulations show that this relaxation time directly determines the experimentally observed decay of the pump–pump photocurrent signal as a function of the delay time. For a heavy hole intersubband spacing of 160 meV, a value of 550 fs was obtained. The experimental method was further applied to determine the LH1–HH1 relaxation time of a second sample with a transition energy below the optical phonon energy. The observed relaxation time of 16 ps

PII: S1367-2630(07)43901-5

is consistent with the value found for the same structure by transmission pump–probe experiments.

The strong need for cheap and integrable Si-based optoelectronic devices for a wide range of applications has been inducing considerable endeavour to develop structures for light emission, modulation and detection in this material system. While recent breakthroughs like the demonstration of a high-speed optical modulator in Si [1] bring the concept of transition from electrical to optical interconnects closer to realization, the base for any silicon photonics, namely a group IV laser source, still waits to be developed. Up to now, the only lasing devices demonstrated in Si are a Raman laser [2] and Si based impurity lasers [3], which essentially lack the advantages associated with the silicon system by requiring an external pump laser source. For silicon as an indirect semiconductor the concept of infrared emitters based on quantum cascade (QC) heterostructures, which is very successfully applied to III–V material systems, provides a promising approach towards a SiGe infrared laser. But despite the successful demonstration of infrared electroluminescence (EL) of various wavelengths for *p*-type SiGe QC structures [4]–[6], lasing has yet to be achieved. The build-up of population inversion in order to achieve lasing fundamentally depends on the relaxation lifetime of the excited energy level of the lasing transition. Therefore the measurement and optimization of the intersubband relaxation time constitutes a key issue for the realization of a Si cascade laser source. The intersubband hole relaxation time for transitions *below* the optical phonon energy (Si–Si : 58 meV, Ge–Ge : 36 meV) is significantly larger than 10 ps and therefore is experimentally well accessible [7]. The lifetimes for energies *above* the optical phonon energies are smaller than 1 ps and are limited by optical deformation potential scattering [8]. So far experiments aimed at the measurement of the lifetime of hole intersubband transitions in this energy range suffered from a lack of time resolution [9] or from hole heating requiring subtraction of heating contributions in order to gain a value for the relaxation time [8].

In this work we present a density matrix (DM) interpretation of the first direct measurement of the excited heavy hole (HH) lifetime in the femtosecond (fs) regime for quantum well (QW) transition energies above the optical phonon energy. A four-level model is presented, which forms the base for the simulation of the time evolution of state occupancies on a fs scale and allows a detailed interpretation of the experimental data. Time resolved measurements were performed using the free electron laser (FEL) FELIX at FOM Rijnhuizen. FELIX provides micropulses with full widths at half maximum (FWHM) down to 280 fs and peak powers of 100 MW. The micropulse repetition rate is 25 MHz, five macropulses of 7 μs duration are provided per second. The FEL power can be reduced to 33 dB by attenuators.

Two samples are investigated in this work. Sample 1 for time resolved measurements at transition energies higher than the optical phonon energy was grown pseudomorphically on a Si [100] substrate at low nominal temperature (350° C). The active region consists of five $Si_{1-x}Ge_x$ valence band QW (widths: 39, 26, 24, 23 and 35 Å; Ge content: 0.42, 0.42, 0.40, 0.37, and 0.28 respectively) and is *p*-type doped (5×10^{17} cm^{-3}). This sequence is repeated ten times and separated by an undoped 500 Å Si barrier. The ten QW periods were sandwiched between 300 nm (100 nm) *p*-type (2×10^{18} cm^{-3}) bottom (top) contacts. X-ray reflectivity measurements show that the actual structural parameters are typically within 1% of the design parameters. The structure was processed into mesa stripes of 7×0.5 mm and contacted with an Al:Si metallization in order to measure the vertical PC. On samples containing similar sets of undoped QW with only a thin barrier between the QW series, QC EL has been observed [4]. Neglecting

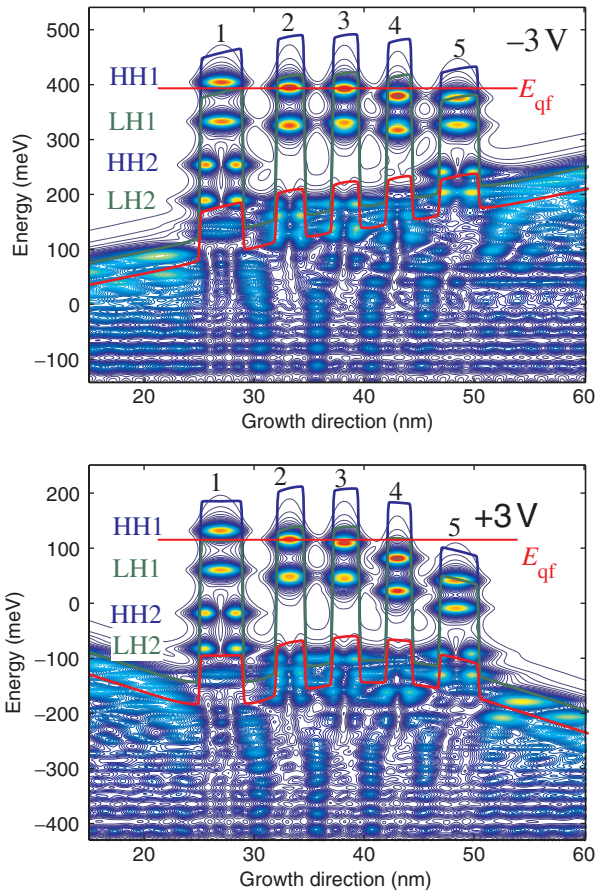

Figure 1. Sample 1: calculated heavy, light and split-off (blue, green, red) hole band edges at a bias of ±3 V and a contour plot of the absolute squared wavefunctions at their eigenenergy values. The calculated HH2–HH1 energy difference of well 1 (160 meV) is consistent with the measurements presented in figure 3. The bandstructure calculations show that the wavefunction overlap between HH1 and HH2 in well 1 does not change significantly when altering the bias voltage. Therefore the relaxation time between those states is stable with respect to a voltage change, which is consistent with the data presented in figure 6. The red line (E_{qf}) indicates the quasi-Fermi level that describes the local equilibrium hole distribution.

the vanishing darkcurrent [10], electrostatically selfconsistent k.p bandstructure calculations have been performed, providing the dipole matrix elements required for the DM simulations. The bandstructure calculations are based on the diagonalization of a 6 × 6 Luttinger–Kohn Hamiltonian and include coupling of the three energetically highest valence bands (HH, light-hole (LH), and split-off (SO) bands) due to finite in-plane wavevectors as well as strain contributions. Further details on the bandstructure simulation are given in [11]. Figure 1 shows the simulation results for the HH, LH and SO band edges for bias voltages of ±3 V. The absolute squares of the wavefunctions are shown as a contour plot, where distribution along the energy axis indicates the energy broadening of the states. The HH1–HH2 transition energy of the deepest well 1 (39 Å, 42% Ge) is calculated to be 160 meV. Sample 2 with transition energies below the optical phonon

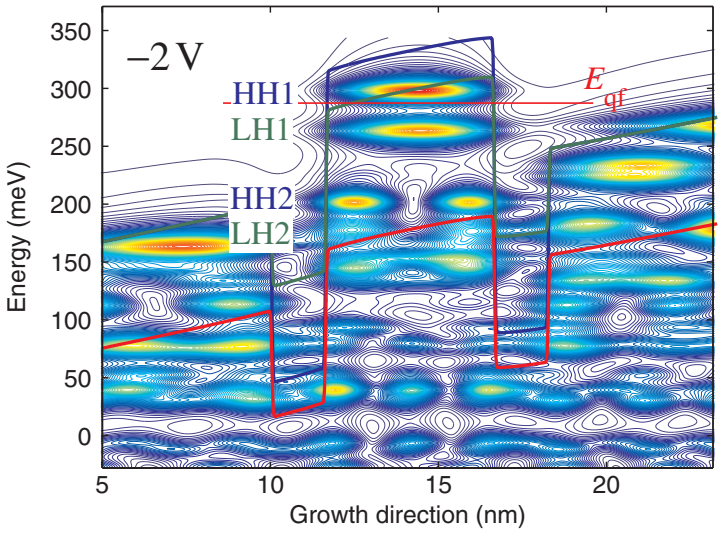

Figure 2. Sample 2: calculated heavy, light and split-off (blue, green, red) hole band edges at a bias of ±3 V and a contour plot of the absolute squared wavefunctions at their eigenenergy values. The calculated LH1–HH1 energy difference is 32 meV, which is below the optical phonon energy. The red line (E_{qf}) indicates the quasi-Fermi level that describes the local equilibrium hole distribution.

energy was grown by MBE on 30% Ge pseudosubstrate. One period of the active region consists of one $Si_{0.67}Ge_{0.33}$ valence band QW with a width of 50 Å and two 16 Å wide $Si_{0.8}Ge_{0.2}$ barriers flanking the well. This *p*-type doped (1×10^{18} cm^{-3}) sequence is repeated 12 times and separated by undoped 100 Å Si barriers. The 12 QW periods were sandwiched between 300 nm (100 nm) *p*-type (2×10^{18} cm^{-3}) bottom (top) contacts. Sample 2 was processed analogue to sample 1. The calculated band structure of sample 2 is shown in figure 2. The HH1–LH1 transition energy is calculated to be 32 meV. For this sample, pump–probe transmission experiments revealed an HH1–LH1 lifetime of 20 ps [12]. Verifying this already determined lifetime by photocurrent (PC) pump–probe experiments aims at directly comparing the results of two different experimental methods and confirming the interpretation of the PC data as a direct monitoring of the excited state population.

Experimentally, the transition energy of sample 1 was determined by voltage modulated waveguide transmission. An externally applied ac voltage (±2 V, 50 kHz) modulated the occupation of the HH1 state, and the resulting change of the spectrally resolved waveguide transmission was measured via lock-in technique for transversal magnetic (TM) radiation. Figure 3(a) shows a clear peak at the calculated HH1–HH2 transition energy. The final HH2 state of this transition is strongly confined. Observing the HH1–HH2 transition of the deepest QW 1 was thus not possible in our previous PC experiments [10], in which low intensity radiation from a globar was used for the excitation of the sample. However, because of the nearly equal spacing in energy of the HH1, HH2 and the onset of the continuum states in well 1, PC can be generated by two photon processes. Figure 3 shows the results of PC experiments making use of the intense laser radiation of FELIX. Figures 3(b) and (c) show a clear two photon PC signal for two different bias voltages resonantly enhanced at the HH1–HH2 transition energy for TM polarization.

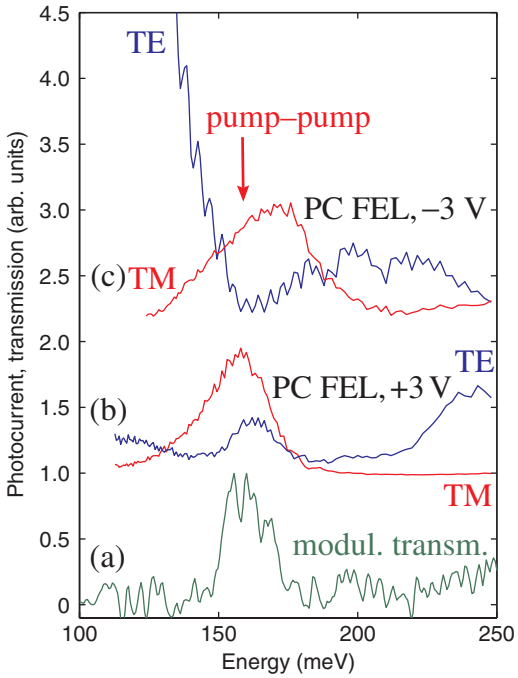

Figure 3. Sample 1: absorption and two-photon PC results. The calculated HH2–HH1 energy difference presented in figure 1 (160 meV) is consistent with the peak positions measured in voltage-modulated TM transmission experiments (a) and in two-photon PC spectra obtained by varying the FEL wavelength (b), (c) for ± 3 V bias). The graphs were offset vertically for clarity. The arrow labelled pump–pump indicates the energy at which the time resolved measurements were performed.

The height of the PC peak induced by a FEL pulse was measured as a function of the FEL micropulse energy for TM polarized radiation in order to verify that a nonlinear absorption process is responsible for the PC signal at the HH1–HH2 energy. For pulse energies smaller than 3×10^{-2} μJ the data presented in figure 4(d) show a clear superlinear dependence of the peak maximum on the pulse energy, which is typical for multi-photon processes. A saturation of the PC signal is observed for pulse energies higher than 5×10^{-2} μJ.

In order to understand the power dependence of the PC signal over the whole range of micropulse energies as well as the dynamics of the state occupancies, the response of the system to a laser pulse resonant with the HH1–HH2 transition was simulated using a DM approach [13, 14]. The processes and states included in this model are depicted in the inset of figure 4(d). The HH1 and HH2 states are labelled by 0 and 1, respectively. The continuum is modelled by two states (2, 3) only. State 2 represents the continuum state that is resonantly coupled to the HH2 state by the radiation field. The relaxation from state 2 into state 3 accounts for the decay from the resonant continuum state into delocalized continuum states not coupled to the QW states by the radiation field but contributing to the measured current. At temperatures small compared to the QW transition energies, the ordinary differential equations describing the time dependence

of the DM elements ρ_{ij} read as follows:

$$
\begin{aligned}
\frac{\mathrm{d}\rho_{00}}{\mathrm{d}t} &= \frac{\rho_{11}}{\tau_{10}} + \frac{\mathrm{i}}{\hbar}eE(t)\mu_{10}\rho_{10} - \frac{\mathrm{i}}{\hbar}eE(t)\mu_{10}\rho_{01},\\
\frac{\mathrm{d}\rho_{11}}{\mathrm{d}t} &= -\frac{\rho_{11}}{\tau_{10}} - \frac{\mathrm{i}}{\hbar}eE(t)\mu_{10}\rho_{10} + \frac{\mathrm{i}}{\hbar}eE(t)\mu_{10}\rho_{01} + \frac{\mathrm{i}}{\hbar}eE(t)\mu_{21}\rho_{21} - \frac{\mathrm{i}}{\hbar}eE(t)\mu_{21}\rho_{12},\\
\frac{\mathrm{d}\rho_{22}}{\mathrm{d}t} &= -\frac{\mathrm{i}}{\hbar}eE(t)\mu_{21}\rho_{21} + \frac{\mathrm{i}}{\hbar}eE(t)\mu_{21}\rho_{12} - \frac{\rho_{22}}{\tau_{32}},\\
\frac{\mathrm{d}\rho_{01}}{\mathrm{d}t} &= -(\Gamma_{10} + \mathrm{i}\omega)\rho_{01} - \frac{\mathrm{i}}{\hbar}eE(t)\mu_{21}\rho_{02} + \frac{\mathrm{i}}{\hbar}eE(t)\mu_{10}\rho_{11} - \frac{\mathrm{i}}{\hbar}eE(t)\mu_{10}\rho_{00},\\
\frac{\mathrm{d}\rho_{02}}{\mathrm{d}t} &= -(\Gamma_{20} + \mathrm{i}2\omega)\rho_{02} - \frac{\mathrm{i}}{\hbar}eE(t)\mu_{21}\rho_{01} + \frac{\mathrm{i}}{\hbar}eE(t)\mu_{10}\rho_{12},\\
\frac{\mathrm{d}\rho_{12}}{\mathrm{d}t} &= -(\Gamma_{12} + \mathrm{i}\omega)\rho_{12} + \frac{\mathrm{i}}{\hbar}eE(t)\mu_{10}\rho_{02} - \frac{\mathrm{i}}{\hbar}eE(t)\mu_{21}\rho_{11} + \frac{\mathrm{i}}{\hbar}eE(t)\mu_{21}\rho_{22},\\
\frac{\mathrm{d}\rho_{33}}{\mathrm{d}t} &= \frac{\rho_{22}}{\tau_{32}}.
\end{aligned}
\tag{1}
$$

Here μ_{ij} denotes the dipole matrix elements between the corresponding states, the Γ_{ij} correspond to the phase relaxation rates and τ_{10} represents the HH2–HH1 energy relaxation time, which is the figure under investigation in this work. Spontaneous relaxation from the continuum states (2, 3) into bound states was excluded, as recapturing of charge carriers from the continuum into the wells appears on a timescale of 5–10 ps, as calculated from the photoconductive gain in [10], and thus far exceeds the temporal width of the laser pulse and the timescale of the experiment.

The model was further simplified by applying the rotating wave approximation [15]. As no coherence effects were observed in the experiment, the time derivatives of the slowly varying components of the off-diagonal elements were set zero (adiabatic approximation). The resulting differential equations relating the diagonal elements of the DM to the temporal envelope of the electromagnetic field (in our case Gauss-shaped) were solved for the intensities shown in figure 4(d) with $\mu_{10} = 2.6$ nm and $\mu_{21} = 1$ nm as calculated from the simulated band structure. For τ_{10} and the FWHM of the laser-pulse the values 550 and 280 fs were used, which have been obtained from the pump–pump experiment discussed in the next section. For the phase relaxation rates, Γ_{12}, Γ_{10}, Γ_{20} a value of 5 THz was used, much faster than any other time constant in the model, since experimentally no coherence effects were observed. This value for the phase relaxation rates corresponds to a homogeneous linewidth of the HH1–HH2 transition one order of magnitude smaller than the absorption linewidth found in figure 3. Note that the absorption width is determined by *inhomogeneous* broadening and thus is expected to be significantly larger than the *homogeneous* linewidth corresponding to Γ_{10}. The relaxation time into state 3 was set equal to the phase coherence time $1/\Gamma_{12}$.

Figure 4 shows the results of the calculation of the time evolution of the occupancies ρ_{00}, ρ_{11} and $\rho_{22} + \rho_{33}$ in figures 4(a)–(c), respectively, for several micropulse energies. Experimentally, the current pulse induced by the FEL micropulse is measured as a voltage drop over a 50 Ω resistor parallel to the input of a voltage amplifier. An estimation of the response of the external electrical circuit to the 300 fs current pulse induced by the FEL radiation shows an initial fast rise of the output voltage with an RC time constant in the 10–50 ns range (determined by

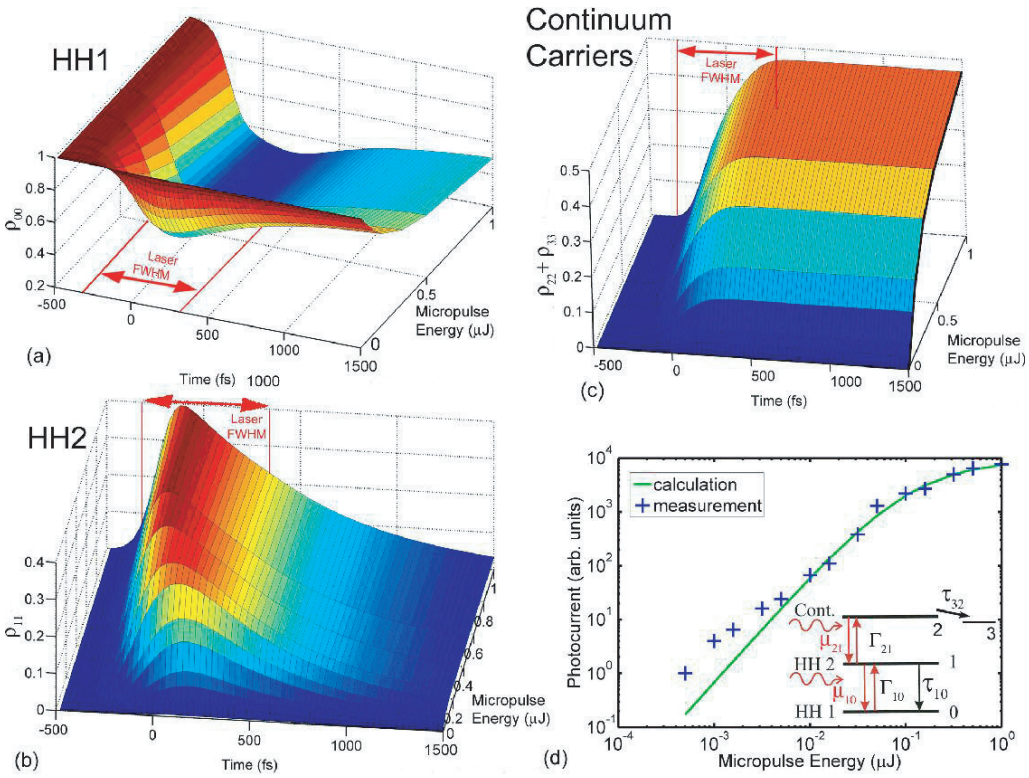

Figure 4. Sample 1: FEL power dependence of the PC signal. Panel (d) shows a double logarithmic plot of the PC signal versus the macropulse power of FELIX. The experimental data (crosses) were measured at a bias of 3 V and a temperature of 10 K in TM polarization. The inset sketches the processes considered in the DM calculations, while the plots (a), (b) and (c) show the calculated time evolution of the HH1, HH2 and continuum state occupancies for a TM polarized laser pulse hitting the sample at $t = 0$. Details of the calculations are given in the text. The calculated dependence of the PC is shown as solid line in plot (d) and is proportional to the number of continuum carriers at the end of the laser pulse as shown in (c).

the capacitance of the device and the 50 Ω input resistor) followed by an exponential decay with the time constant of the preamplifier's low-pass filter ($1 - 10\,\mu$s) that is much larger than the micropulse separation (40 ns). Since the input–output characteristic of the external circuit is linear, the response of the electrical circuit to the *micro*-pulse train that makes up a *macro*pulse is proportional to the sum over N identically decaying exponentials excited at the times $t_{0,\ldots,N-1}$ at that the N micropulses hit the sample, provided that the sample relaxes to its equilibrium states between subsequent micropulses (from previous experiments, it is known that this occurs on a 10 ps timescale [10]). In our experiment, we integrate the amplifier output over a FEL macropulse by a box-car integrator. Following the preceding discussion it is evident, that this integral is proportional to the system response to a single micropulse, which in turn is proportional to the carriers excited into the continuum during one micropulse. Therefore, in figure 4(d) the experimental values for the PC signal are compared to calculated ones of $\rho_{22}(t_e) + \rho_{33}(t_e)$ at a time $t_e = 1.5$ ps larger than the pulsewidth but smaller than the decay time

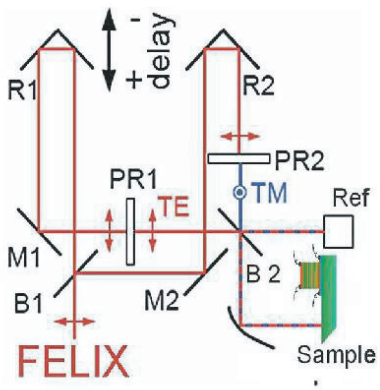

Figure 5. Pump–pump set-up. The FEL beam with a wavelength of 7.9 μm enters the optical set-up in transverse electric (TE) polarization and is splitted by a beam splitter (B1). The polarization of one of the beams is turned by 90° into transverse magnetic (TM) polarization (PR2). The beam remaining in TE polarization is reflected by a movable mirror (R1) allowing to adjust the delay between TE and TM pulse on a fs scale. Before being coupled into the sample waveguide, the beams are made collinear again by the use of a second beam splitter (B2). The integral PC through the variably biased sample originating from the delayed TE and TM micropulses is measured as a function of the delay.

of continuum states. The calculation is in very good agreement with the measurement over two orders of magnitude of the exciting power. The calculations show, that for low excitation intensities HH2 is only weakly populated by the pulse, most carriers remain in HH1. Therefore the continuum occupation depends quadratically on the intensity. As the peak intensity gets higher, the HH1–HH2 transition reaches bleaching (i.e. the HH1 and HH2 populations become equal) within the pulse time, and therefore the continuum occupation and the PC become linearly dependent on the excitation intensity. For even higher intensities, the occupations of HH1, HH2 and continuum become comparable, thus the transition to the continuum becomes bleached and the PC saturates.

The DM calculations are used to precisely describe the processes involved in PC pump–pump experiments aimed at quantifying the HH2–HH1 relaxation time, which has been reported to be mainly determined by optical phonon deformation potential scattering [8, 16].The pump–pump set-up is shown in figure 5. The advantage of PC measurements over pump–probe experiments lies in their much higher sensitivity. In addition, major set-up problems of pump–probe transmission experiments in waveguide configuration, like distinguishing between the parallel pump and probe beams, are avoided. The cross-polarization of the FEL beams introduces an asymmetry into the experiment with respect to the sign of the delay, and allows an unambiguous identification of decay processes even if the decay time constant is close to the time resolution of the set-up. Furthermore it prevents the two beams from interfering.

Figure 6 compares the experimental results with the simulation. The black curves present the PC signal after subtracting a background corresponding to large delays. The green line represents the simulation results, which were obtained by introducing two beams in polarization vector notation into the DM calculation and performing the simulation of the time evolution for

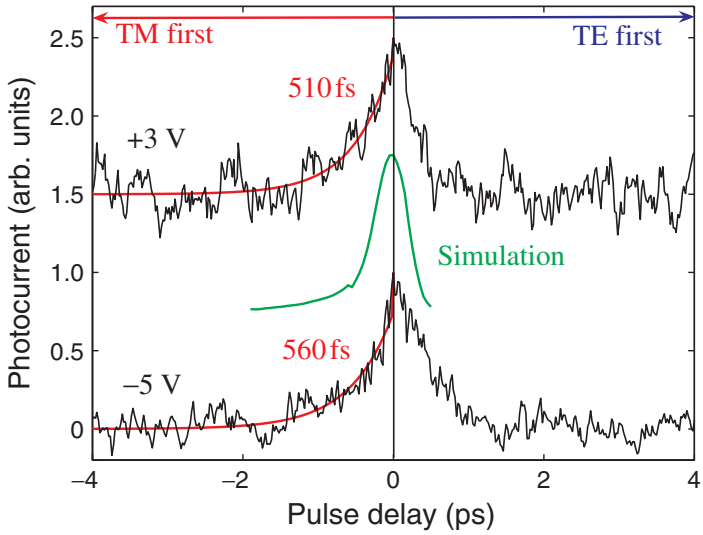

Figure 6. Sample 1: plot of the PC as a function of the delay between the TM and TE pump pulses for different bias voltages. A constant background equivalent to the current-integral over the two non-interacting pulses has been subtracted and the traces have been offset vertically for clarity. The FEL macropulse power was 160 μJ (TM) and 130 μJ (TE) attenuated by 5 dB for a bias of −5 V and 120 μJ (TM) and 160 μJ (TE) attenuated by 20 dB for 3 V bias. An exponential fit results in an HH2–HH1 relaxation time of 510 ± 60 fs for +3 V and 560 ± 18 fs for −5 V (red lines). Also shown is the result of pump–pump simulations (green line) using the same parameters as in the simulation of the power PC dependence on the micropulse energy shown in figure 4(d).

the various delays displayed in figure 6. In the simulations, the HH2–HH1 relaxation time τ_{10} was used as a fitting parameter. With $\tau_{10} = 550$ fs an excellent agreement between measured and simulated results was obtained (see figure 6). Moreover, with this value for τ_{10} also the power dependence of the PC can be accurately modelled over three decades of micropulse powers (see figure 4(d)). This finding strongly suggests that all relevant processes are included in the simulation and that the extraction of the parameters, most interestingly the HH intersubband relaxation time, is performed correctly. The interpretation of the experimental data is based on the picture presented in figure 4. The strong asymmetry of the curves in figure 6 with respect to the sign of the delay is due to the strong polarization dependence of the transition involved. Negative delays in figure 6 present results for cases, in which the TM polarized pulse is the first to interact with the sample. In TM polarization the HH1–HH2 transition is allowed, and thus a non-equilibrium population of the HH2 state will build up. This non-equilibrium HH2 occupation decays exponentially with the time constant τ_{10}, as presented in figure 4(b). From the HH2 state, holes can be excited to the continuum also in TE polarization. Therefore, if the TE pulse hits the structure before the HH2 carriers have relaxed, the integral PC increases proportionally to the residual holes in the HH2 state. Thus the measured decay of the integral PC change as a function of the pulse delay directly monitors the HH2 lifetime, allowing the extraction of the HH2–HH1 relaxation time by performing an exponential fit for the data in figure 6 gained at negative delays. In TE polarization, HH1–HH2 transitions are forbidden at the Γ point and become only weakly

allowed for HH1 vectors with finite momentum perpendicular to the growth direction. Thus only negligible HH2 populations can be excited from the HH1 ground state by a TE pulse. As a consequence, the HH2 relaxation cannot be observed if the TE pulse arrives first (positive delays in figure 6), resulting in an asymmetry with respect to the pulse order as observed in the experiment. The fast decaying increase of the PC signal between 0 and 1.5 ps in figure 6 results from the overlap of the TE and TM pulse, and thus indicates the time-resolution of the experimental set-up. The extracted HH2–HH1 relaxation time of 550 fs is significantly longer than the time resolution of the measurement set-up.

As already mentioned, our simulation accurately reproduces the experimental results for both kinds of measurements, where the use of one consistent set of parameters, one of which is the hole intersubband relaxation time, implies a fundamental understanding of the processes involved in the experiments. The extracted HH2–HH1 subband relaxation time τ_{10} is thus highly reliable. The experiment was performed for several bias voltages. However, within the experimental error of the lifetimes $3\sigma = 60$ fs for +3 V and 18 fs for -5 V no dependence of the lifetime on the applied bias could be observed. We believe that this is due to the fact, that according to the band structure calculations presented in figure 1 the wavefunction overlap of the HH2 and HH1 states of the deepest QW 1 does not change when altering the voltage within the range investigated in the experiments.

We report a significantly longer relaxation time (550 fs) than reported in [8] (250 fs), where a contribution of hole heating had to be deconvoluted in order to gain this value. In our experiment, such heating effects would only enter via a time-dependent development of the distribution function for the *excited* HH2 population into a Fermi–Dirac distribution described by an elevated hole temperature and a HH2 quasi-Fermi level. Calculations indicate a decrease of the HH2-continuum absorption at the pump–pump wavelength of 7.9 μm as a consequence of heating. Thus, a deviation from exponential decay and an *underestimation* of the HH2 relaxation time would result due to heating. However, we want to point out that due to the low excitation intensity sufficient for our experiments, no deviations from an exponential HH2 decay could be observed. Also in previous work, under the higher intensities required for pump–probe absorption determinations of lifetime, only the heating of the HH1 *ground* state distribution was subtracted in the analysis and the influence of a hot HH2 excited state distribution was neglected [8].

To further confirm experimentally that PC pump–pump experiments probe the excited state lifetime, we compare time resolved pump–pump measurements on sample 2, for which a HH1–LH1 transition time of 20 ps was reported in [12], with conventional pump–probe experiments in transmission at photon energies below the optical phonon energy. Figure 7 shows the result of PC pump–pump measurements at a FEL wavelength of 37.9 μm, a macropulse energy of 70 μJ and an attenuation of 13 dB (red line), where the FEL beams hit the sample surface normally (both beams TE polarized, but cross-polarised). The side peaks found in the experimental data at $\pm$15 ps originate from the overlap of the second beam with the fraction of the first beam reflected by the sample's back surface. The 15 ps delay are consistent with the sample thickness of 600 μm. The reflection of the first pulse is included in the fit presented in figure 7, which reveals a HH1–LH1 relaxation time of 16 ps in good agreement with the value of 20 ps reported in [12]. Due to the absence of any long-term decay as present in the pump–probe transmission experiments reported in [12], the relaxation time fit in figure 7 can be performed over double the time range in comparison to the data in [12], while the signal-to-noise ratio is comparable. PC pump–pump experiments performed at a FEL wavelength of 36 μm also

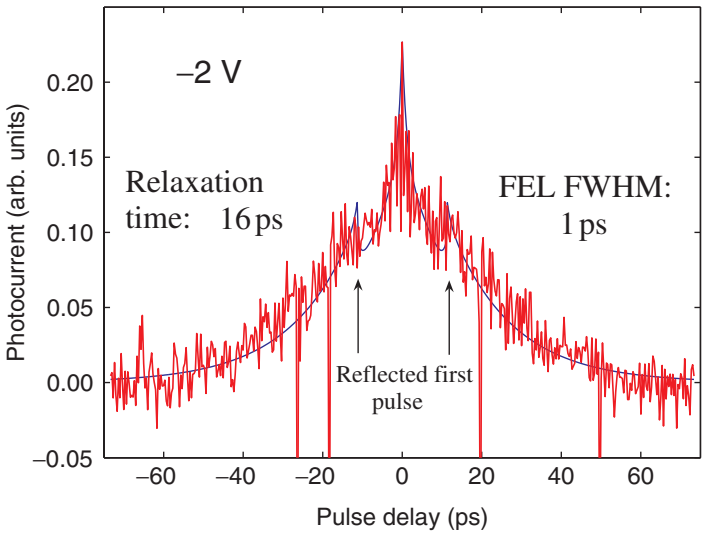

Figure 7. Sample 2: plot of the PC as a function of the delay between the two TE pump pulses (red line). A constant background equivalent to the current-integral over the two non-interacting pulses has been subtracted. The FEL macropulse power was 70 μJ attenuated by 13 dB for a bias of −2 V. The side peaks at ±15 ps are due to the reflection of the first FEL pulse at the sample's back surface and are included in the fit by introducing a second overlap peak of equal shape and decay as the central peak. The exponential fit of the decay reveals an LH1–HH1 relaxation time of 16 ps (blue line), where the FEL pulse FWHM is 1 ps.

revealed a lifetime of 15 ps indicating that boron absorption at 35.9 μm does not influence the result of the PC pump–pump measurements.

To summarize, in this work we presented a DM interpretation of experimental data, which to our knowledge enable the first *direct* determination of the intersubband hole relaxation time for transitions above the optical phonon energy in the SiGe material system. Due to the consistency achieved in modelling and experiment, the HH2–HH1 lifetime, that for sample 1 is limited by the optical deformation potential scattering [8], is highly reliable and can be extracted directly from the observed decay of the pump–pump signal as a function of the delay between TM and TE pulses. In our experiment, we obtained 550 fs for this lifetime, approximately two times larger than reported previously [8]. In addition, the experiment described in this work in principle allows the measurement of the excited state lifetime of a QCL structure. A direct comparison of PC pump–pump measurements with pump–probe experiments in transmission was accomplished by verifying the LH1–HH1 relaxation time of sample 2 reported in [12]. The value of 16 ps for the relaxation time of sample 2 lies in the experimentally well accessible time range of transition energies below the optical phonon energy. As our experiments were not restricted to this time range and were performed on biased devices, our results constitute a key step in the design and dynamic simulation of SiGe QC laser structures. Pump–pump PC measurements on sample 2 confirmed the LH1–HH1 relaxation time with a transition energy below the optical phonon energy determined in transmission pump–probe experiments in [12].

Acknowledgments

We gratefully acknowledge the support by the Stichting voor Fundamenteel Onderzoek der Materie (FOM) in providing the required beam time on FELIX and highly appreciate the skilful assistance of the FELIX staff. This work was supported by the European Community Research Infrastructure Action under the FP6 'Structuring the European Research Area' Programme through the Integrated Infrastructure Initiative 'Integrating Activity on Synchrotron and Free Electron Laser Science', by the EC (IST-2001-38035) and by the FWF (F2512-N08) and GME, both Vienna and Austria.

References

[1] Liu A, Jones R, Ling L, Samara R, Rubin D, Cohen O, Nicolaescu R and Paniccla M 2004 *Nature* **427** 615
[2] Boyraz O and Jalali B 2004 *Opt. Express* **12** 5269
[3] Pavlov S, Huebers H and Ruemmeli M H 2002 *Appl. Phys. Lett.* **80** 4717
[4] Dehlinger G, Diehl L, Gennser U, Sigg H, Faist J, Ensslin K, Grützmacher D and Müller E 2000 *Science* **290** 2277
[5] Bormann I, Brunner K, Hackenbuchner S, Zandler G, Abstreiter G, Schmult S and Wegscheider W 2002 *Appl. Phys. Lett.* **80** 2260
[6] Lynch S, Bates R, Paul D, Norris D, Cullis A, Ikonic Z, Kelsall R, Harrison P, Arnone D and Pidgeon C 2002 *Appl. Phys. Lett.* **81** 1543
[7] Kelsall R *et al* 2005 *Phys. Rev.* B **71** 115326
[8] Kaindl R, Wurm M, Reimann K, Woerner M, Elsaesser T, Miesner C, Brunner K and Abstreiter G 2001 *Phys. Rev. Lett.* **86** 1122
[9] Boucaud P, Julien F, Prazeres R, Ortega J, Sagnes I and Campidelli Y 1996 *Appl. Phys. Lett.* **69** 3069
[10] Rauter P, Fromherz T, Bauer G, Diehl L, Dehlinger G, Sigg H, Grützmacher D and Schneider H 2003 *Appl. Phys. Lett.* **83** 3879
[11] Fromherz T, Koppensteiner E, Helm M, Bauer G, Nützel J and Abstreiter G 1994 *Phys. Rev.* B **50** 15073
[12] Pidgeon C, Phillips P, Carder D, Murdin B, Fromherz T, Paul D, Ni W-X and Zhao M 2005 *Semiconductor Sci. Technol.* **20** L50
[13] Mukamel S 2005 *Nonlinear Optical Spectroscopy* (London: Oxford University Press)
[14] Rulliere C 1998 *Femtosecond Laser Pulses* (Berlin: Springer)
[15] Yarif A 1989 *Quantum Electronics* (New York: Wiley)
[16] Ikonic Z, Harrison P and Kelsall R 2001 *Phys. Rev.* B **64** 245311